HOUSING FLEXIBILITY EFFECTS ON ROTOR STABILITY

L. B. Davis, E. A. Wolfe,
and R. F. Beatty

Rockwell International/Rocketdyne Division
Canoga Park, California

Abstract

Rotordynamic analyses have typically considered only the rotating assembly and in the last 10 years have been expanded to include housing dynamics. Advanced rotating machinery designs conceptually define the rotor well ahead of the housing. Preliminary rotordynamic evaluations are performed with a housing stiffness assumption that is typically determined only after the hardware is built. In addressing rotor stability, a rigid housing assumption has shown to predict an instability at a lower spin speed than a comparable flexible housing analysis. This rigid housing assumption therefore provides a conservative estimate of the stability threshold speed. A flexible housing appears to act as an energy absorber and dissipates some of the destabilizing force. The fact that a flexible housing is usually asymmetric and considerably heavier than the rotor has been related to this apparent increase in rotor stability. Rigid housing analysis is proposed as a valuable screening criteria and may save a significant amount of time and money in construction of elaborate housing finite element models for linear stability analyses.

Introduction

A primary consideration for high-pressure turbomachinery such as used in liquid rocket engines is minimum weight. To achieve this while delivering the pressures and flows required by the system, the design trend is toward small diameters and very high speeds. The results of this trend are rather spectacular as shown in Fig. 1. As an example, the Space Shuttle

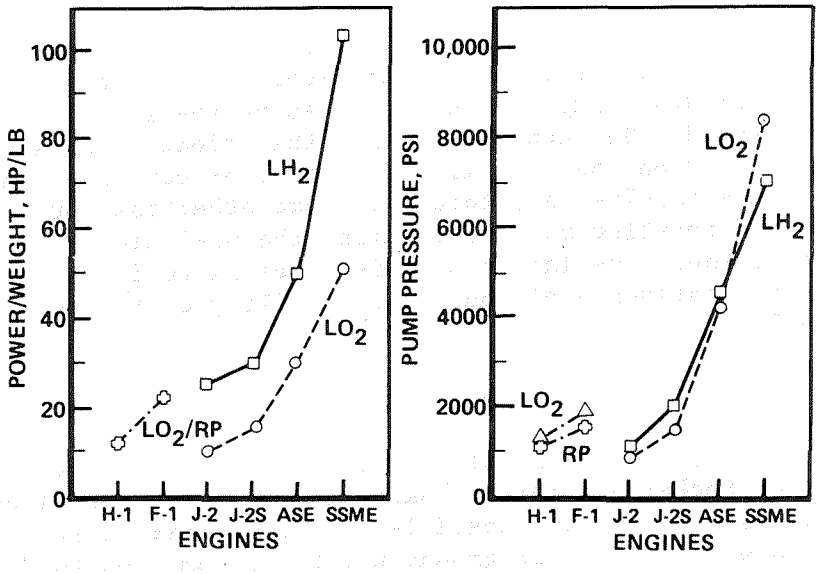

Fig. 1. Turbopump Power Growth

Main Engine High-Pressure Fuel Turbopump (SSME HPFTP) is one of the most advanced machines in the world with a power density of 100 horsepower/pound. While there is a substantial weight savings in the rotor with its small diameter, much of the savings is associated with the lightweight housing. A lightweight housing is designed primarily as a pressure shell with a minimum of additional structure added to support the rotor. At high speeds, housing motion becomes a significant feature affecting rotor critical speeds, stability, and bearing loads.

Housing designs are dictated by pressure, flow, hydrodynamic efficiency, structural loads, and assembly requirements. While low speed pumps with massive and stiff housings are generally used to discuss rotating machinery problems, advanced lightweight housings are not as simply treated. The flexibility of the housing, coupled through bearings and seals, results in a considerably more complex problem, which is not as amenable to simple rules of design as in the past. Rotor stability is much more difficult to accurately predict today due to the added variable of housing

dynamics and the interaction with the coupling mechanisms. These elements affect critical speeds and thus the rotor stability for operation above the rotor critical speed. The concern is with the effect of housing flexibility on the stability analysis, or can more conservative results be obtained in some other fashion for advanced rotating machinery during the preliminary study phase. The intent of this paper is to investigate the influence of housing flexibility on the rotor stability.

Approach

Initially, the housing dynamics influence on several of Rocketdyne rotordynamic analyses was determined. To accomplish this, compatible stability cases were repeated with a rigid or ground housing assumption to quantify the change in threshold speed with elimination of housing flexibility and dynamics. A total of six different turbopump designs were included in this survey including four SSME designs and two advanced rocket engine designs. The specific turbopumps included were:

1. High-pressure oxygen turbopump (HPOTP) of the SSME
2. Uprated high-pressure oxygen turbopump of the SSME for full power operation, referred to as the HPOTP Phase II
3. High-pressure fuel (liquid hydrogen) turbopump (HPFTP) of the SSME
4. MK38-0 redesign configuration that never materialized for a modified SSME
5. MK48-F high pressure fuel (liquid hydrogen) turbopump for the Orbital Transfer Vehicle (OTV)
6. MK49-F high pressure fuel (liquid hydrogen) turbopump for the Advanced Space Engine (ASE)

These six turbopump analyses were chosen because each has a detailed finite element model of its housing. The

following is a brief description of each of the turbopumps included in the survey.

The HPOTP is shown in Fig. 2 and a summary of its performance characteristics is provided in Table 1. Basically, the HPOTP consists of a double-entry centrifugal impeller supplying liquid oxygen to the main chamber. A portion of this discharge flow is diverted to a smaller centrifugal impeller mounted on the same shaft that supplies liquid oxygen to the preburners. A two-stage impulse turbine, which overhangs the bearings, drives the pump to a maximum operating speed of 27,900 rpm. Two pairs of duplex angular contact ball bearings support the rotor. Preload springs between the bearing outer races in each pair maintain the axial load independent of rotor axial position. The turbine hot gases are isolated from the pump by a series of floating ring seals. Axial thrust on the rotor is reacted by a double-balance piston built into the main impeller.

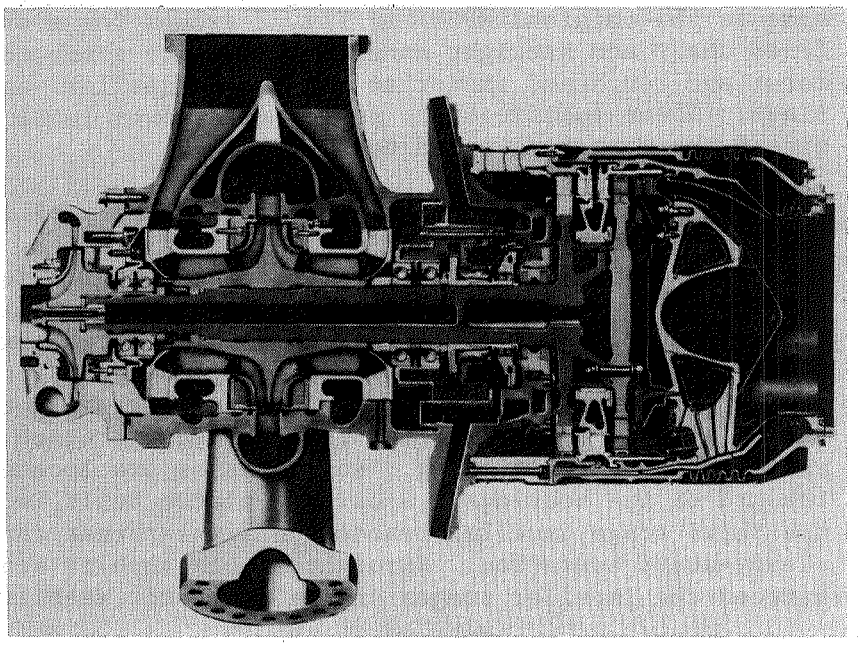

Fig. 2. High-Pressure Oxygen Turbopump

Table 1. SSME HPOTP PERFORMANCE DATA

KEY PERFORMANCE PARAMETERS BASELINE DATA JAN. 1984				
	RPL		FPL	
	MAIN	BOOST	MAIN	BOOST
PUMP INLET FLOWRATE, LB/SEC	1070.6	111.6	1157.8	129.4
PUMP INLET PRESS, PSIA	379.3	3985.9	392.4	4403.6
PUMP DISCHARGE PRESSURE, PSIA	4108.7	7106.7	4556.0	7861.2
PUMP EFFICIENCY	0.684	0.809	0.650	0.800
TURBINE FLOWRATE, LB/SEC	61.8		69.0	
TURBINE INLET PRESSURE, PSIA	5015.3		5660.8	
TURBINE INLET TEMP, R	1407.2		1596.3	
TURBINE PRESS RATIO	1.506		1.550	
TURBINE EFFICIENCY	0.749		0.755	
TURBINE SPEED, RPM	27102		29675	
TURBINE HORSEPOWER	22902		29174	

The uprated HPOTP Phase II design is basically the same as the original HPOTP of Fig. 2 except for a stiffened shaft and straight annular seals with a smooth rotor and roughened stator at the small impeller wear rings. These modifications permit full power level and extend the operating speed to 30,000 rpm.

The HPFTP is shown in Fig. 3 and a summary of its performance characteristics is provided in Table 2. The HPFTP consists of a three-stage centrifugal (liquid hydrogen) pump driven by a two-stage turbine to deliver the engine coolant. The turbopump operates at a maximum speed of approximately 37,000 rpm. Two pairs of duplex angular contact ball bearings support the rotor radially and a thrust bearing is provided for start and shutdown axial positioning. Rotor masses are located inboard of the bearings. A balance piston built into the third stage impeller reacts the axial thrust during steady-state operation. Straight smooth annular seals between the impeller stages ensure the rotor stability.

The MK38-0 redesign configuration included was a proposed concept for upgrading of the SSME to increase its thrust rating. Basically, this design has a direct

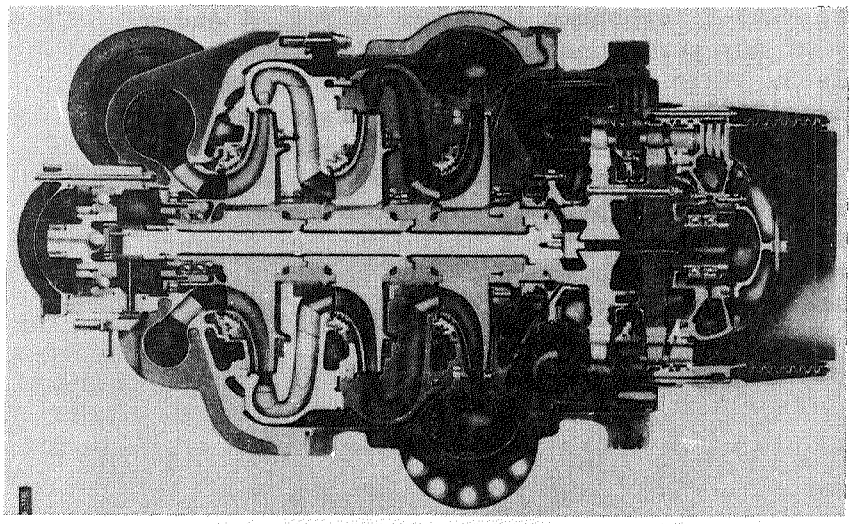

Fig. 3. SSME High-Pressure Fuel Turbopump

Table 2. SSME HPFTP Performance Data

KEY PERFORMANCE PARAMETERS	RPL	FPL
PUMP INLET FLOWRATE, LB/SEC	148.4	161.7
PUMP INLET PRESSURE, PSIA	204.1	214.0
PUMP DISCHARGE PRESSURE, PSIA	6254.8	7036.8
PUMP EFFICIENCY	0.758	0.757
TURBINE FLOWRATE, LB/SEC	147.5	164.0
TURBINE INLET TEMPERATURE, R	1898.4	1989.2
TURBINE PRESSURE RATIO	1.522	1.558
TURBINE EFFICIENCY	0.770	0.780
TURBINE SPEED, RPM	34,931	37,076
TURBINE HORSEPOWER	63,288	77,142

drive, two-stage turbine and two centrifugal impellers mounted on a shaft supported by angular contact ball bearings. The maximum operating speed is approximately 26,000 rpm.

The MK48-F turbopump is shown in Fig. 4 and a summary of its performance characteristics is provided in Table 3. This turbopump consists of a three-stage centrifugal (liquid hydrogen) pump driven by a two-stage overhung turbine. The pump design is similar to the HPFTP on a much smaller scale and has a maximum operating speed of approximately 95,000 rpm. Again, two pairs of angular contact ball bearings support the rotor radially and a balance piston built into the third stage impeller reacts the axial thrust.

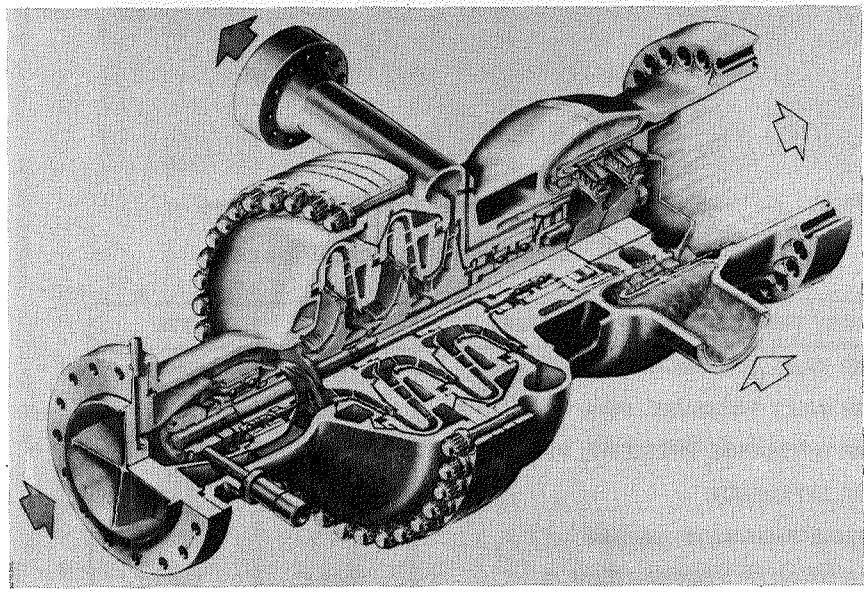

Fig. 4. MK48-F Liquid Hydrogen Turbopump

Table 3. MK48-F Performance Data

KEY PERFORMANCE CHARACTERISTICS	
FLOWRATE, GPM	628
DISCHARGE PRESSURE, PSI	4,560
DESIGN SPEED, RPM	95,000
TURBINE POWER, HP	2,543
WEIGHT, POUNDS	105

The MK49-F turbopump is shown in Fig. 5 with a performance characteristic summary given. This turbopump is very similar to the MK48-F but on a slightly smaller scale. The MK49-F has a maximum operating speed of 110,000 rpm and relies on straight smooth interstage seals to ensure the rotor stability.

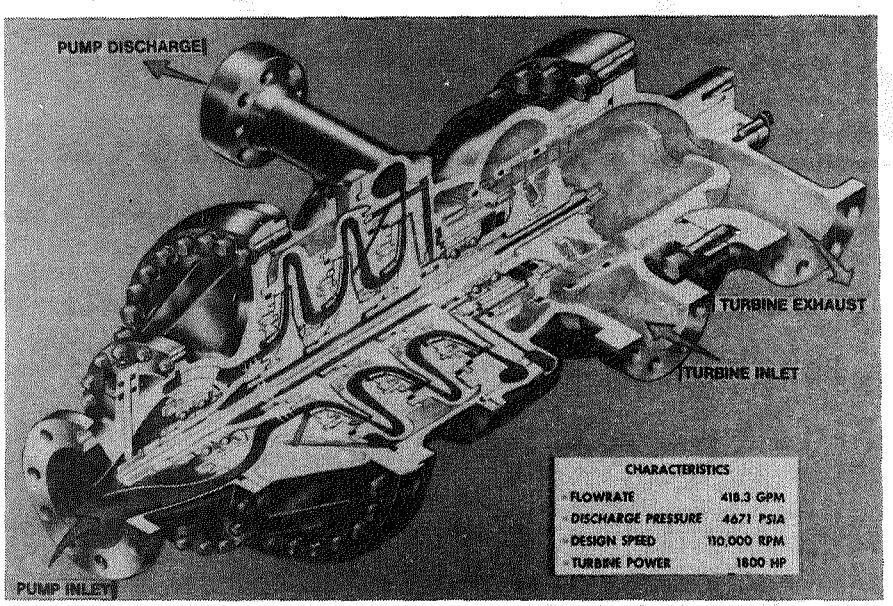

Fig. 5. MK49-F Liquid Hydrogen Turbopump

Mathematical Models Description

Existing finite element models of the rotor and housing for each of the six turbopumps included in the survey were used. The rotors are constructed of beam finite elements and the housings are typically composed of plate elements to include shell motion. Typical rotor and housing finite element models are shown in Fig. 6 and 7, respectively, for the SSME HPOTP. The coupled system was analyzed using modal synthesis techniques that combine substructures of the rotor and housing-to-engine support structure connected through linear bearings, seals, and hydrodynamic interactions. This approach has been described by Childs (Ref. 1) for rotordynamics applications. Generally, the housing-to-engine

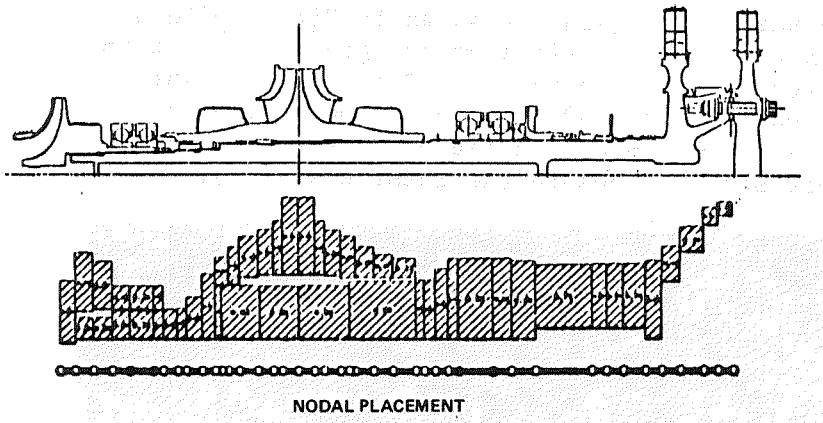

Fig. 6. SSME HPOTP Rotating Assembly Finite Element Model

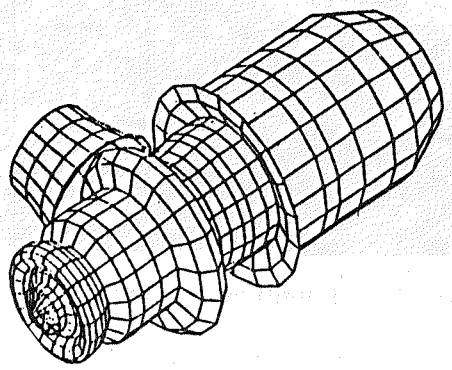

Fig. 7. SSME HPOTP Housing Finite Element Model

support structure is unsymmetric and is lightly damped. These linear models not only include bearing and seal coupling but also, impeller diffuser interaction, turbine aerodynamic cross coupling, bearing damping, and rotor and housing structural damping. Output capability includes damped critical speeds and stability.

Stability Calculations

The Rocketdyne internal stability criterion is similar to that of Lund (Ref. 2) and Bansal (Ref. 3), which considers a mechanical system at steady-state

which undergoes a perturbation. The motion takes one of three forms. When the deviation from the original motion decreases with time, the system is stable. If the deviation increases with time, the system is said to be unstable. Neutral stability occurs when the motion of the system after a perturbation is oscillatory with no change in amplitude with time.

The equation of motion for a typical mechanical system takes the following form:

$$m\ddot{y} = -ky - c\dot{y} + F(t) \tag{1}$$

Assume the solution to the homogeneous differential equation is as follows:

$$y = \tilde{Q}e^{\lambda t} \tag{2}$$

substituting into the equation of motion:

$$m\lambda^2 + c\lambda + k = 0 \tag{3}$$

where the eigenvalue is:

$$\lambda = \frac{-c \pm \sqrt{c^2 - 4km}}{2m} \tag{4}$$

$$\lambda = -a \pm bi \tag{5}$$

where:

$$a = \frac{c}{2m} \qquad b = \frac{\sqrt{4km - c^2}}{2m}$$

Writing the general solution to the homogeneous equation of motion:

$$y = Q_1 e^{(-a + bi)t} + Q_2 e^{(-a - bi)t} \tag{6}$$

$$y = e^{-at}\left(Q_1 e^{bit} + Q_2 e^{-bit}\right) \tag{7}$$

Using Euler's formula, equation (7) can be rewritten in the general solution form:

$$y = e^{-at} [A\cos(bt) + B\sin(bt)] \qquad (8)$$

Plotting the solution:

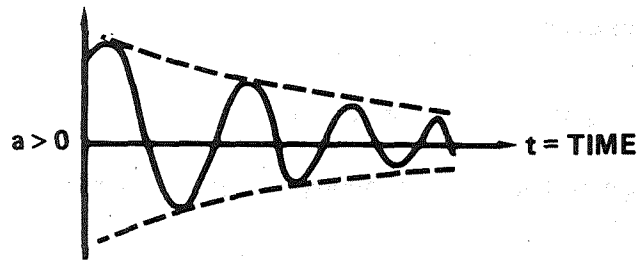

Fig. 8. Rate of Amplitude Change (a > 0)

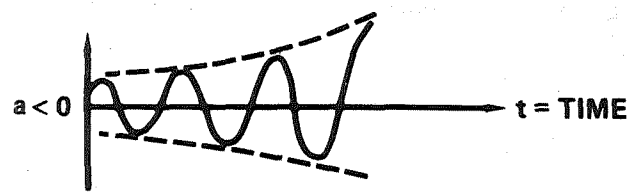

Fig. 9. Rate of Amplitude Change (a < 0)

Figure 8 displays decreasing amplitude with time, and therefore a stable system for a > 0. However, when the real part of λ is greater than zero, the system is unstable. This unstable motion is represented in Fig. 9. Lastly, if a = 0, the e^{-at} term becomes unity and the amplitude remains constant with time, as shown in Fig. 10. Therefore, the sign of the real part of the eigenvalue determines the stability of the system.

Fig. 10. Rate of Amplitude Change (a = 0)

Stability Results of Survey

As previously mentioned, the stability results of a rigid versus a flexible housing assumption were compared. Figures 11 through 17 present rotor stability

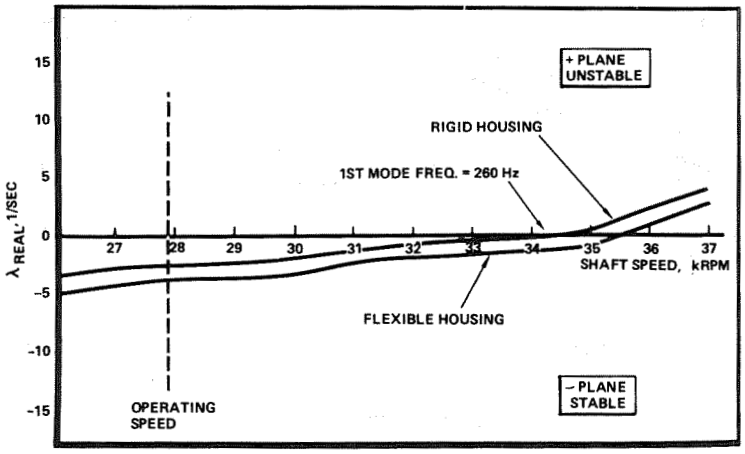

Fig. 11. HPOTP Stability Map of Turbine Overhang Mode (Hot Gas Seals Free to Float)

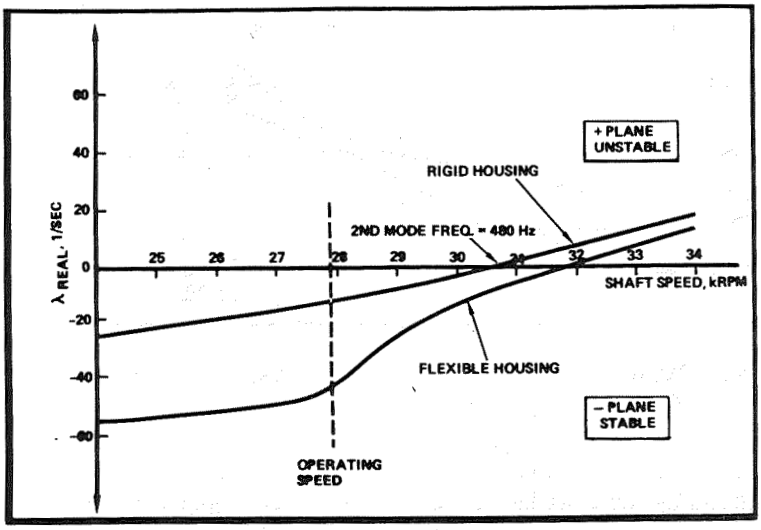

Fig. 12. HPOTP (104%) Rotor Stability Map (Second Rotor Mode)

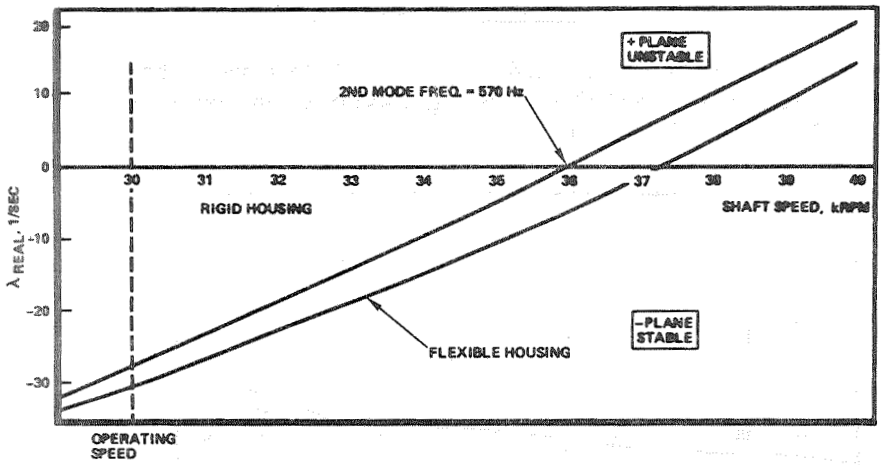

Fig. 13. HPOTP (109%) Rotor Stability Map (Second Rotor Mode)

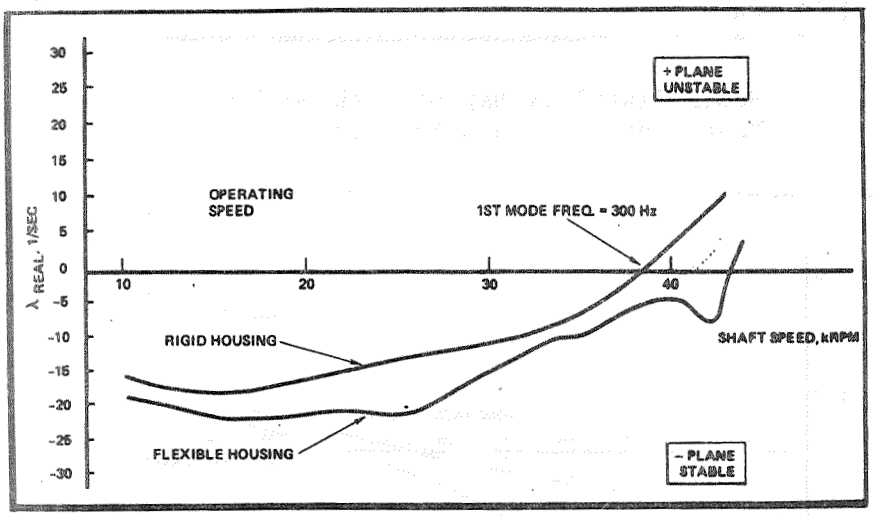

Fig. 14. MK38-0 (Redesign) Rotor Stability Map (1st Rotor Mode)

maps for each of the six turbopumps described for only the potentially unstable modes. The real part of the complex eigenvalue is plotted as a function of the rotor spin speed where a positive real part eigenvalue indicates the potential for unstable rotor motion to occur.

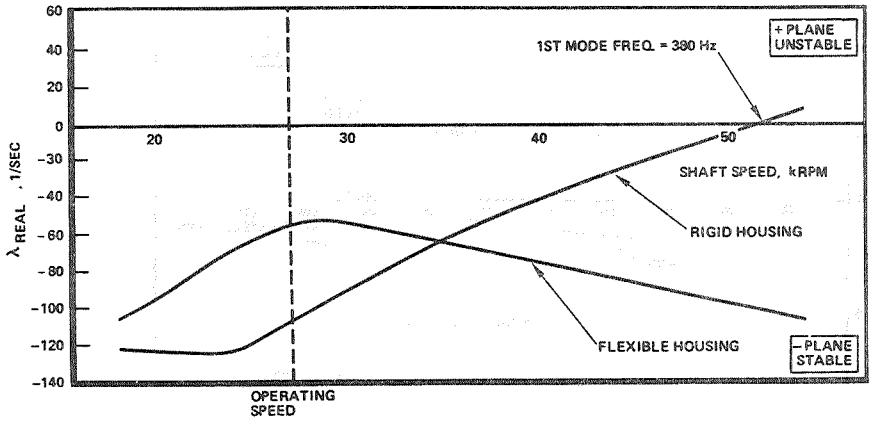

Fig. 15. HPFTP Rotor Stability Map (First Rotor Mode)

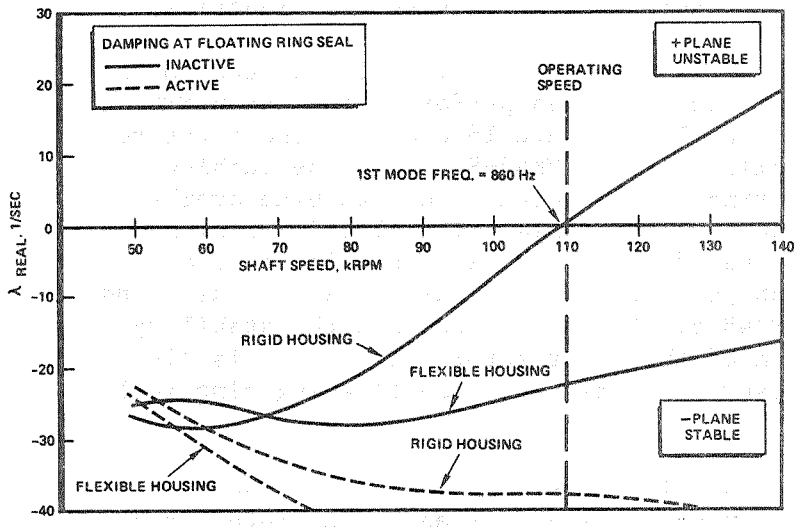

Fig. 16. MK49-F Rotor Stability Map (First Rotor Mode)

Figure 11 compares the lowest rotor mode stability of the HPOTP, which is the turbine overhang mode. With the hot gas seals free to float, the operating speed is far removed from the stability threshold speed for both a rigid and a flexible housing. A comparison of the second rotor mode stability of the HPOTP is shown in Fig. 12 and 13, which is the main impeller mode. Figure 14 compares the turbine overhang mode for the MK38-0

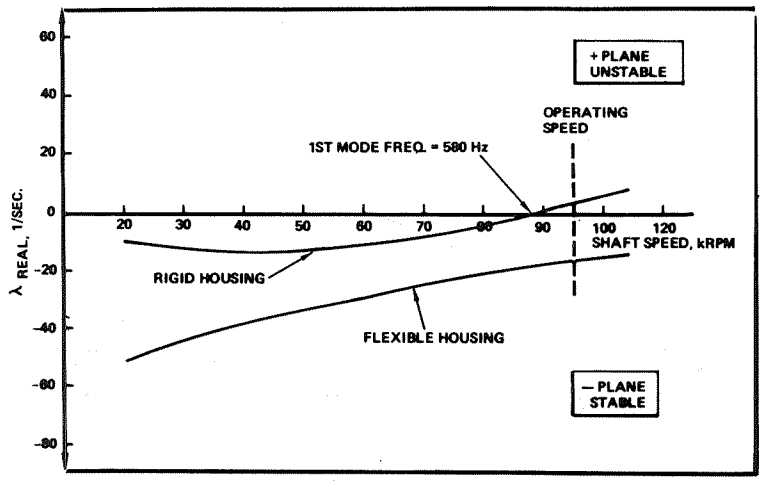

Fig. 17. MK48-F Rotor Stability Map (1st Rotor Mode - Floating Ring Seal Inactive)

redesign configuration. A comparison of the lowest rotor mode stability was performed for the HPFTP as shown in Fig. 15. Figure 16 compares the first rotor mode stability of the MK49-F. With the turbine floating ring seals present, this turbine overhang rotor mode remains stable. The floating ring seal was deactivated to produce an unstable rotor mode for comparison purposes. A similar situation was found for the MK48-F. Figure 17 presents the stability comparison of the first rotor mode, which is also a turbine overhang mode, with the floating ring seal inactive.

The stability maps described above indicate that as the rotor spin speed increases, the rotor in a flexible housing tends to approach an unstable condition at a higher speed than the rotor in a rigid housing. This observation is true for all six turbopumps. Thus, results of the survey to determine the effect of housing flexibility on rotor stability indicate that a rigid housing assumption is more conservative since it consistently predicts lower threshold speeds. It appears as though the housing acts as an energy absorber. This can be seen when it is considered that the housing adds relative motion terms.

Consider the following:

$$q_R = A\cos\omega t + B\sin\omega t$$

$$q_S = C\cos\omega t + D\sin\omega t$$

The elastic coupling force between the rotor and support is:

$$F = -(kq + c\dot{q}) = -[k(q_R - q_S) + C(\dot{q}_R - \dot{q}_S)]$$

The work, or energy, generated per cycle is:

$$W = \int_0^{2\pi} \left\{-[k(q_R - q_S) + c(\dot{q}_R - \dot{q}_S)] \cdot \dot{q}_R\right\} \frac{d(\omega t)}{\omega}$$

Rearranging the above equation as follows:

$$W = \int_0^{2\pi} [-(kq_R + c\dot{q}_R)] \cdot \dot{q}_R \frac{d(\omega t)}{\omega}$$

$$-\int_0^{2\pi} [-(kq_S + c\dot{q}_S)] \cdot \dot{q}_R \frac{d(\omega t)}{\omega} \cdot$$

Therefore it follows that if the housing support was rigid or ground, then q_S and $\dot{q}_S$ are zero. All the constant available energy in a conservative system is then transmitted to the rotor and none dissipated in the housing. It follows then that a flexible housing absorbs some of the energy that would normally be present in the rotor.

Another aspect of housing construction that aids stability is its typical asymmetry. Several technical papers discuss bearing support asymmetry related to stability gain. Most turbopumps are unsymmetrically supported by manifolds, ducts, and brackets. This can be illustrated simply (Fig. 18) by representing a

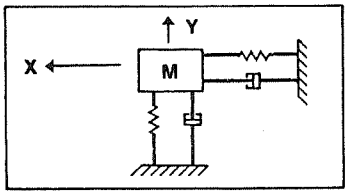

UNSYMMETRIC MODES

$K_{xx} \neq K_{yy}$

$C_{xx} \neq C_{yy}$

Fig. 18. Simple Housing Model

housing as a mass attached to ground with two radial degrees of freedom relative to the centerline as shown below. The equations of motion for Fig. 18 are:

$$\begin{bmatrix} M & 0 \\ 0 & M \end{bmatrix} \begin{Bmatrix} \ddot{x} \\ \ddot{y} \end{Bmatrix} + \begin{bmatrix} c_{xx} & c_{xy} \\ c_{yx} & c_{yy} \end{bmatrix} \begin{Bmatrix} \dot{x} \\ \dot{y} \end{Bmatrix}$$

$$+ \begin{bmatrix} k_{xx} & k_{xy} \\ k_{yx} & k_{yy} \end{bmatrix} \begin{Bmatrix} x \\ y \end{Bmatrix} = \begin{Bmatrix} 0 \\ 0 \end{Bmatrix}$$

Assuming harmonic motion solution and appropriate derivations of:

$$\begin{Bmatrix} x \\ y \end{Bmatrix} = \begin{Bmatrix} X \\ Y \end{Bmatrix} e^{\lambda t}$$

give the following solution:

$$\begin{Bmatrix} X \\ Y \end{Bmatrix} \left(\begin{bmatrix} M & 0 \\ 0 & M \end{bmatrix} \lambda^2 + \begin{bmatrix} c_{xx} & c_{xy} \\ c_{yx} & c_{yy} \end{bmatrix} \lambda \right.$$

$$\left. + \begin{bmatrix} k_{xx} & k_{xy} \\ k_{yx} & k_{yy} \end{bmatrix} \right) = \begin{Bmatrix} 0 \\ 0 \end{Bmatrix}$$

Reformating the solution yields:

$$\begin{vmatrix} (M\lambda^2 + c_{xx}\lambda + k_{xx}) & (c_{xy}\lambda + k_{xy}) \\ (c_{yx}\lambda + k_{yx}) & (M\lambda^2 + c_{yy}\lambda + k_{yy}) \end{vmatrix} = 0$$

The stability can be investigated by the Routh-Hurwitz criterion (Ref. 4) as follows. The characteristic equation is:

$$a_0\lambda^4 + a_1\lambda^3 + a_2\lambda^2 + a_3\lambda + a_4 = 0$$

where assuming $c_{xy} = c_{yx} = 0$, the coefficients for the above equation are:

$$a_0 = M^2$$

$$a_1 = M(c_{xx} + c_{yy})$$

$$a_2 = (k_{yy}M + k_{xx}M + c_{xx}c_{yy})$$

$$a_3 = (c_{xx}k_{yy} + c_{yy}k_{xx})$$

$$a_4 = (k_{xx}k_{yy} - k_{xy}k_{yx})$$

The system is stable if the following quantities are greater than zero:

$$D_1 = a_1$$

$$D_2 = \begin{vmatrix} a_1 & a_0 \\ a_3 & a_2 \end{vmatrix}$$

$$D_3 = \begin{vmatrix} a_1 & a_0 & 0 \\ a_3 & a_2 & a_1 \\ 0 & a_4 & a_3 \end{vmatrix}$$

$$D_4 = a_4 D_3$$

Substituting the above equations and expanding yields

$$D_1 = M(c_{xx} + c_{yy})$$

$$D_2 = M^2(c_{xx}k_{xx} + c_{yy}k_{yy}) + M(c_{xx}^2 c_{yy} + c_{xx}c_{yy}^2)$$

$$D_3 = c_{xx}c_{yy}M^2 (k_{xx} - k_{yy})^2 + k_{xy}k_{yx}M^2 (c_{xx} + c_{yy})^2$$
$$+ Mc_{xx}c_{yy} (c_{xx}^2 k_{yy} + c_{xx}c_{yy}k_{yy} + c_{xx}c_{yy}k_{xx}$$
$$+ c_{yy}^2 k_{xx})$$

$$D_4 = (k_{xx}k_{yy} - k_{xy}k_{yx}) D_3$$

Note that, since k_{xx}, k_{yy}, c_{xx}, and c_{yy} are usually greater than zero, the possibility for a system instability generally is controlled by the D_3 quantity. Therefore, in a symmetric case if $k_{xy} = -k_{yx}$, the system stability tends to decrease. However, if asymmetry exists then $k_{xx} \neq k_{yy}$ and the first term on the righthand side of the equation is positive and the trend is for stability to increase. Since the rotor response is relative to the housing and the housing stability is increased, then the rotor/housing system must follow. This stability criterion cannot predict the magnitude of the gain because in reality there are several coupling mechanisms that vary in some fashion with shaft speed. It was therefore necessary to construct a simple generic turbopump model where some of these ideas can be more easily evaluated.

Generic Turbopump Model

A model was constructed to simulate a typical turbopump with attention given to significant dynamic features. The finite element model consists of 10 lumped mass and inertia locations for both the rotor and housing. Three large masses reside at appropriate locations in the rotor model to analytically represent two impellers and a turbine disk. A description of the model is provided in Fig. 19.

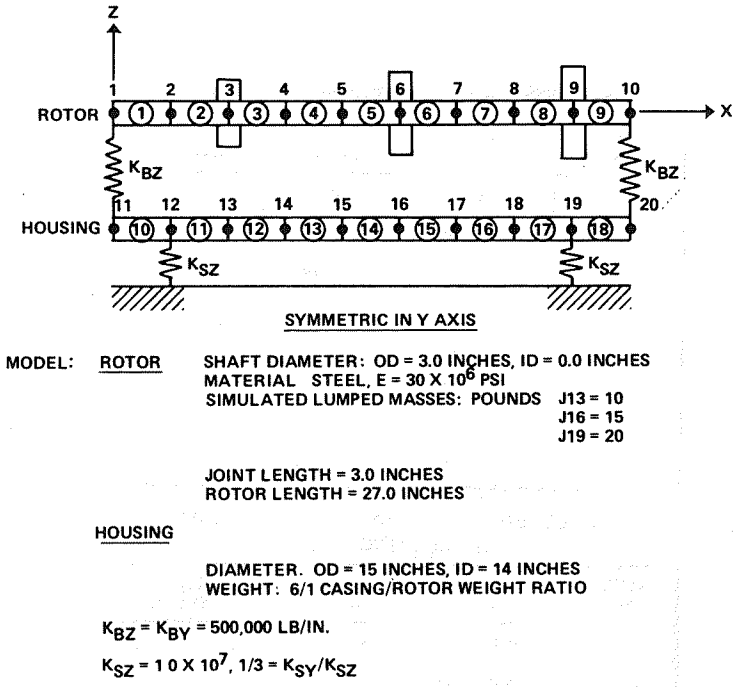

Fig. 19. 20 Lumped Mass Turbopump Model

Inputs to the analysis included mass and stiffness properties that were selected to be a generic representation of a turbopump. In addition, rotor/housing coupling coefficients for the HPOTP were arbitrarily selected as typical. These coefficients included the wear ring seal coupling on the first disk, the impeller-diffuser interaction on the second disk, and the turbine interstage seal coupling coefficients on the third disk. These coefficients are provided in Table 4.

To further study rotor stability with a flexible housing, several dynamically important parameters were varied. The weight of the housing was varied from one to seven times the weight of the rotor. A housing/rotor weight ratio of approximately 6:1 is typical of many existing turbopumps as shown in the data of

Table 4. Generic Turbopump Model Rotor/Housing Coupling Coefficients

WEAR RING SEAL COUPLING ON FIRST DISK

SPEED, RPM	K_{xx}, LB/IN.	K_{xy}, LB/IN.	C_{xx}, LB-SEC/IN.
1,000	0.	0.	0.
10,000	1.0×10^5	1.5×10^4	6.3×10^1
20,000	4.2×10^5	5.8×10^4	—
25,000	6.5×10^5	8.6×10^4	—
30,000	9.3×10^5	1.2×10^5	2.1×10^2
35,000	1.2×10^6	1.6×10^5	—
40,000	1.6×10^6	2.0×10^5	—
45,000	2.1×10^6	2.7×10^5	3.2×10^2

IMPELLER – DIFFUSER INTERACTION ON SECOND DISK

SPEED, RPM	K_{xx}, LB/IN.	K_{xy}, LB/IN.	C_{xx}, LB-SEC/IN.
1,000	-8.9×10^1	-4.0×10^1	0.1
10,000	-8.9×10^3	-4.0×10^3	1.0
20,000	-3.5×10^4	-1.6×10^4	2.0
25,000	-5.5×10^4	-2.5×10^4	2.5
30,000	-8.0×10^4	-3.6×10^4	3.0
35,000	-1.1×10^5	-4.9×10^4	3.5
40,000	-1.4×10^5	-6.4×10^4	4.0
45,000	-1.8×10^5	-8.1×10^4	4.5

TURBINE INTERSTAGE SEAL COUPLING ON THIRD DISK

SPEED, RPM	K_{xx}, LB/IN.	K_{xy}, LB/IN.	C_{xx}, LB-SEC/IN.
1,000	0.	0.	0.
10,000	8.7×10^3	1.9×10^3	2.3
20,000	3.5×10^4	7.9×10^3	6.1
25,000	4.7×10^4	1.3×10^4	8.8
30,000	6.8×10^4	2.1×10^4	12.8
35,000	9.5×10^4	3.1×10^4	17.3
40,000	1.3×10^5	4.6×10^4	23.0
45,000	1.6×10^5	6.4×10^4	29.6

Table 5. Since the significant dynamic difference between a rigid and flexible housing is asymmetric modes and with insight provided by Ref. 5 , the effects of support asymmetry was determined by varying the support

Table 5. Housing/Rotor Weight Ratio of Existing Turbopumps

MODEL	ROTOR WEIGHT, POUNDS	HOUSING WEIGHT, POUNDS	HOUSING/ROTOR WEIGHT RATIO
MK38-O (104%)	81.	480.	6/1
MK38-O (109%)	81.	480.	6/1
MK38-F	128.5	649.	5/1
MK48-F	8.25	87.75	10/1
MK49-F	6.1	48.	8/1

stiffness ratio in orthogonal directions. Figure 20 shows the stability threshold speed plotted as a function of the support asymmetry ratio for a family of housing/rotor weight ratios. Results show that there is an optimum value of asymmetry that produces the

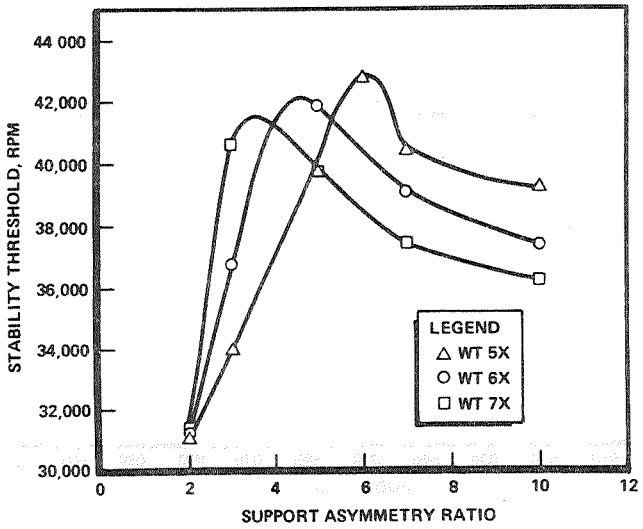

Fig. 20. 20 Lumped Mass Model (Stability Threshold vs Support Asymmetry Ratio)

maximum stability threshold speed for a given housing/rotor weight ratio. This optimum asymmetry ratio varies as the housing/rotor weight ratio is increased. The larger the housing/rotor weight ratio, the smaller the optimum asymmetry ratio to produce a maximum threshold speed. For example, an asymmetry ratio of 3:1 produces the highest threshold speed for a large housing/rotor weight ratio, whereas an asymmetry ratio of 10:1 requires a low weight ratio to produce the highest threshold speed.

Finally, housing modal damping was varied to determine its effect on rotor stability. The modal damping (percentage of critical damping) supplied by the housing structure was varied with increasing asymmetric support ratios. Figure 21 shows that as the housing modal damping is increased, the stability threshold speed remains nearly constant. This result does not change with the housing/rotor weight ratio.

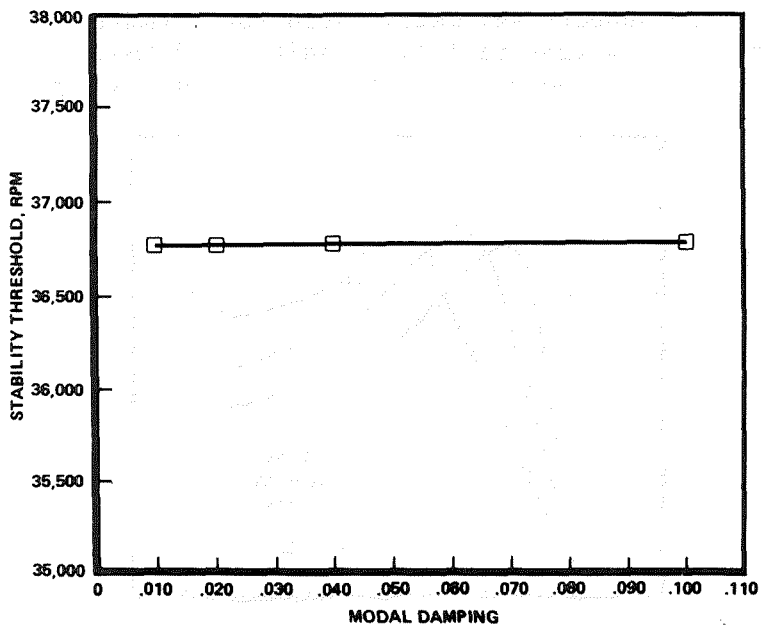

Fig. 21. Modal Damping vs Stability Threshold (20 Lumped Mass Model)

In an effort to compare the previously observed trends of the six turbopumps to this generic model, stability analyses using both a rigid and flexible housing assumption were performed. Figure 22 shows a stability map for the simple model. The flexible housing approaches an unstable condition at a higher speed than the rotor in a rigid housing. This result emulates the turbopump survey performed earlier. The analysis was performed with the typical 6:1 housing/ rotor weight ratio and a support asymmetry ratio of 3:1.

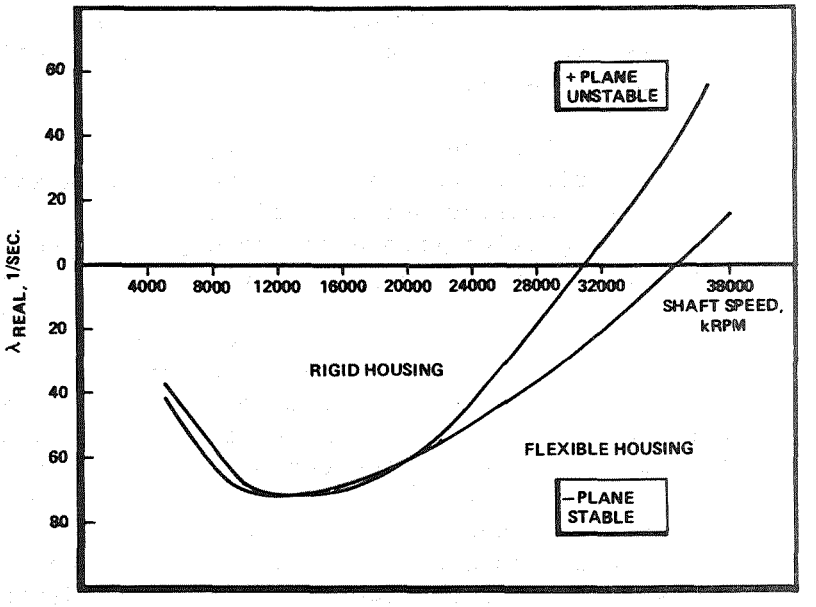

Fig. 22. Generic Turbopump Model Stability Map

Conclusions and Recommended Design Practice

A rotor stability analysis with a rigid housing assumption predicts an instability at a lower speed compared to a similar flexible housing case. Consequently, a rigid housing assumption is more conservative for design than the flexible model. Simple analysis approaches indicate that a flexible housing acts as an inefficient energy absorber and dissipates only a small portion of the destabilizing

forces in the rotor/housing system. The significant stability improvement associated with a housing is attributed to asymmetric supports. In a simple generic turbopump model, it was determined that the asymmetric support stiffness ratio grounding the housing should be greater than a value of 2:1. This simple model also indicated the optimum housing asymmetric support ratio is dependent on the housing/rotor weight ratio. Review of the weight data for the stable turbopumps included in the survey and the weight parametric study indicate most well behaved pumps have or should have at least a 5:1 housing to rotor weight ratio. Housing structural damping variations indicate no significant effect on the rotor stability.

For future designs, these results indicate some general rules to act as guidelines. These include: asymmetric housing supports of greater than a 2:1 ratio and heavier than a 5:1 housing to rotor ratio. Also, preliminary analyses should predict conservative stability results assuming a rigid housing depending on the accuracy of the coefficients that couple the rotor to the housing. Based on analytic results, in many cases complex housing models are not necessary for stability analyses. As a result, time and money are saved in the development of rotordynamic models.

Housing models would be required if detailed response analyses are necessary, however, the variation in response with unknown rotor unbalance distributions many times makes preliminary response work unreliable. In practice, a high-speed rotor balance in the housing is recommended to obtain minimal response.

Nomenclature

A,B = constants, determined by initial conditions

c = damping, lb-sec/in.

F = excitation force, pounds

k = stiffness, lb/in.

m,M = mass, lb-sec^2/in.

$Q, Q_{1,2}$ = arbitrary constants

q_R = rotor displacement, inches

$\dot{q}_R$ = rotor velocity, in./sec

q_S = housing displacement, inches

$\dot{q}_S$ = housing velocity, in./sec

t = time, seconds

W = work per cycle, lb-in./cycle

ω = spin speed, rad/sec

y = displacement, inches

$\dot{y}$ = velocity, in./sec

$\ddot{y}$ = acceleration, in./sec^2

References

1. Childs, Dara, "Simulation Models for Flexible Spinning Bodies," Transactions of the ASME, November 1975.

2. Lund, J. W., "Stability and Damped Critical Speeds of a Flexible Rotor in Fluid Film Bearings, Journal of Engineering for Industry, May 1975.

3. Bansal, P. N., "Stability and Damped Critical Speeds of Rotor-Bearing Systems," Journal of Engineering for Industry, November 1975.

4. Wylie, Advanced Engineering Mathematics, McGraw-Hill, p. 613, 1960.

5. Gunter and Trumple, "The Influence of Internal Friction on the Stability of High Speed Rotors With Axistropic Supports, Journal of Engineering for Industry, p. 1105, November 1969.